DETECTION OF, AND COMMUNICATION WITH SPACE VEHICLES DURING ATMOSPHERIC ENTRY; PROBLEMS IN SIMULATION

by

S. C. Lin*

Avco-Everett Research Laboratory

INTRODUCTION

In considering the problem of communicating with outer space and detection of spacecraft from the ground, one usually has to worry about only the propagation characteristics of electromagnetic waves of vacuum wavelength falling within either one of the two well known "atmospheric windows," namely; (1) the "optical window" extending from about 0.3 microns to a few microns, and (2) the "RF window" extending from a few millimeters to about 30 meters in the wavelength scale. However, during entry (or reentry) of a spacecraft into the earth's atmosphere, there exists two physical phenomena which tend to complicate the communication problem on the one hand, and to simplify the detection problem on the other hand.

To explain these phenomena, let us take a look at the hypersonic flow field around a typical vehicle depicted in Figure 1. This schematic drawing is reproduced from a paper published by Professor Lester Lees of California Institute of Technology in 1962 (Ref. 1). Even though a sphere is used here as an example for the sake of simplicity, the

---

* Now Professor of Engineering Physics, University of California, at San Diego, La Jolla, California.

general features of the flow field are quite characteristic of those of the hypersonic flow around a realistic spacecraft, such as the Mercury capsule and the planned Apollo re-entry vehicle. As noted by Professor Lees, one of the most striking features of the flow field around such a blunt object at hypersonic speed is the bow shock wave. This shock wave, nearly parabolic in shape, is first formed in front of the re-entering spacecraft at altitudes of the order of 300,000 to 400,000 ft, depending on the size of the spacecraft. The gas that traverses the strong, nearly normal portion of the bow shock wave, is compressed and heated irreversibly by the shock, and forms an outer wake behind the body. The temperature and density of the gas behind the apex of the bow shock wave, where the gas is practically stagnant, is illustrated in Fig. 2. This figure is reconstructed from a paper by B. Kivel, dated 1959.[2] The temperature and density shown here as functions of flight velocity and altitude were based on a local equilibrium adiabatic shock compression process. The dotted lines illustrated some typical velocity-altitude relationships for two typical spacecrafts during re-entry; namely, a Mars probe and a near-orbit earth satellite. It is seen that the gas temperature in the stagnation region, that is, the region behind the apex of the bow shock wave, is typically of the order of 6,000 to 15,000°K. After the shock compression, the gas re-expands as it accelerates around the side of the spacecraft so that the temperature in the other part of the flow field may be expected to be somewhat lower. However, even after isentropic expansion back to ambient pressure, which occur in a distance of about 50 to 100 diameters behind the spacecraft, the gas temperature would still remain at about 4500°K at satellite velocity and at about 7000°K at the Mars probe velocity. At these high

temperatures, air, which is normally transparent through the visible part of the spectrum, becomes highly dissociated, ionized and optically active. This is illustrated in Fig. 3 and 4, which depict the chemical composition of air behind the normal shock wave up to satellite velocity, and the spontaneous emission intensity up to 18,000°K temperature under the condition of thermodynamic equilibrium. Since this emitted radiation, which amounts to many kilowatts or even megawatts per liter of the high temperature air, is given out mostly in the visible part of the spectrum, it becomes a bothersome background noise when one tries to communicate with a spacecraft through the "optical window" of the atmosphere. On the other hand, this strong radiation also serves as a natural beacon announcing the arrival of the spacecraft as it enters the earth's atmosphere. An example of this phenomenon is illustrated in Fig. 5, which shows a ballistic camera trace of a missile nose cone as recorded by the Avco Everett Research Laboratory over the south Atlantic.[4] This photograph was taken with an open shutter camera in much the same way as in the recording of luminous meteor trails.

The second physical phenomenon which complicates the communication problem of hypersonic flight is the ionization phenomenon. At satellite velocity, the degree of ionization behind a normal shock under the conditions of thermodynamic equilibrium is about 0.1%. At higher velocities, the degree of ionization is correspondingly higher (see Fig. 6 and Ref. 5). Even at the degree of ionization of 0.1%, the high temperature air is already a better conductor of electricity than sea water by a factor of about 100. In terms of number of free electrons present, a 0.1% ionization corresponds to 5×10^{13} electrons per cubic centimeter behind a bow shock at an altitude of 40 miles. This is about 10^8 times

greater than the maximum electron density found in the ionosphere. Thus, a re-entering satellite would soon find itself engulfed in a plasma sheet which is practically impenetrable to radio frequency electromagnetic radiation. This gives rise to the so-called "communication black-out" phenomenon, which normally occupies the essential part of the re-entry period.

Even though the thermal ionization phenomenon just mentioned does not make the gas emit strongly in the radio frequency part of the electromagnetic spectrum, it nevertheless manifests itself in the detection problem in another way; namely, as the ionized gas expands around the side of the spacecraft into the wake, the electrons that are produced by the bow shock wave do not disappear immediately. Instead, they recombine at a finite rate and hence persist over considerable distances behind the spacecraft. For spacecrafts of sufficiently large sizes, the wake flow often becomes turbulent even at relatively high altitudes (see Refs. 1 and 6). As the ionized gas produced by the bow shock wave is inhomogeneously mixed with the cold ambient air in the turbulent flow field, the resultant gas mixture becomes a very good scatterer of radio frequency electromagnetic radiation.[7] This is illustrated in Fig. 7, which shows the strong radio echoes observed by Lin, Goldberg, and Janney[8] during re-entry of the MA-6 Mercury capsule carrying Lt. Col. John Glenn in his first orbital flight on February 20, 1962. The radio frequency employed in this case was 30 Mc/S and the altitude of the Mercury capsule during the observation was about 230,000 ft. For several seconds before and after the Mercury capsule passed overhead the observation station, the equivalent back-scattering cross section of the turbulent wake of the Mercury capsule was found to be several

thousand times greater than the bare-body cross section of the Mercury capsule itself in free space.

COMMUNICATIONS THROUGH IONIZED SHOCK LAYERS AND WAKES

With the above introductory remarks, we shall now examine the fundamental problems related to the radiation and ionization phenomena. In particular, we shall try to identify the various physical quantities which govern the absolute intensities of these phenomena. In view of the fact that the problems of communication through the optical window and through the RF window of the atmosphere are somewhat different (even though the fundamental processes are somewhat related), we shall consider these two problems separately. Here we are using the word "communication" in a somewhat general sense to include both the problems of detection and of signal-sending.

Communication Through the Optical Window: The problem of communication through the optical window invariably involves the question of absolute spectral emissivity of the high temperature air produced in a hypersonic flow field. A typical set of emission spectra from shock-heated air, nitrogen and oxygen is illustrated in Fig. 8. It is seen that the spectra generally consist of intense molecular bands, atomic lines, and continua of various origins which spread over the major portion of the visible spectrum. In the problem of detection of spacecraft during re-entry, one is most interested in those parts of the spectrum where the emission is the strongest in order to select the most suitable optical sensor. On the contrary, in the signal-sending problem, one is

interested in the other parts of the spectrum where the emission is the weakest so that the background noise within the communication channel (e.g., a narrow-band laser beam) can be avoided as much as possible. In this latter problem, one is also interested in knowing the absorption coefficient of the high temperature gas in the same spectral region, so that the sending of optical signals through the shock layer can be made with a minimum amount of attenuation.

In order to determine the absolute spectral emissivity and absorbtivity in the various parts of the hypersonic flow field, it is necessary first of all to know the thermodynamic state of the gas in the various parts of the flow field. Secondly, one has to know all the chemical kinetic processes which determine the relative concentration of the different chemical species which participate in the emission and absorption processes. (This includes also the excitation and de-excitation mechanisms of the various energy states for each chemical species.) Finally, after knowing the relative population of the various energy states of the different chemical species, one needs to know further the absolute optical transition probabilities associated with various molecular bands and atomic lines.

Communication Through the RF Window: Due to the great disparity between the atomic length scale and the wavelength of radio frequency electromagnetic waves, the bound states of atoms and molecules generally do not absorb strongly in the radio frequency part of the electromagnetic spectrum. Therefore, the communication problem through the RF window essentially involves the presence of free electrons in the high temperature gas.

The problem of propagation of radio waves through an ionized medium

has been a subject of intense study at the turn of this century by physicists and geophysicists, such as Lorentz, Appleton, Chapman, Sellmeyer, Heavyside, Hartree and others.[10, 11] More recently, this has also been a subject of intense study by plasma physicists,[12, 13] but in this latter case the interest has mainly been centered around the problems of wave propagation and emission in a highly ionized gas in the presence of a strong magnetic field. In the present discussion, however, it suffices to go back to the classical dispersion formulae as derived by Lorentz and others to illustrate the point.

The propagation of a plane wave of amplitude $\underset{\sim}{E}$ in a dispersive medium can in general be represented by the following equation:

$$\underset{\sim}{E} = \underset{\sim}{E}_o \exp[i(\omega t - \gamma \frac{z}{\lambda_o})] \tag{1}$$

where

$$\gamma = n - ik = (\varepsilon - i \frac{4\pi\sigma}{\omega})^{1/2} \tag{2}$$

in the complex propagation constant; ω is the angular frequency; and $\lambda = C/\omega$ is the free-space wavelength dived by 2π. The real part of the propagation constant n, known as the "refractive index." determines the velocity of propagation; while the imaginary part k, known as the "extinction coefficient," determines the rate at which the amplitude of the electromagnetic wave attenuates with distance along the direction of propagation z. The refractive index n and the extinction coefficient k are in turn related to the dielectric constant ε and the electrical conductivity σ through the second half of Eq. (2). For an ionized gas in the absence of a strong magnetic field, the dielectric constant and the electrical conductivity are respectively given

by (according to Lorentz, as modified by Sellmeyer, see Ref. 9)

$$\varepsilon = 1 - \frac{\omega_p^2}{\omega^2 + \nu^2} \tag{3}$$

$$4\pi\sigma = \frac{\omega_p^2 \gamma}{\omega^2 + \nu^2} \tag{4}$$

In the above expression, ω_p is the angular plasma frequency, which is linearly proportional to the square root of the number density of free electrons n_e, such that (e being the electron charge, and m_e being the electron mass)

$$\omega_p^2 = \frac{4\pi e^2}{m_e} n_e \tag{5}$$

The quantity ν , known as the electron collision frequency, on the other hand, is a complicated averaged quantity which measures the rate of damping of the organized electron motion due to collisions with the gas molecules, atoms and positive ions.[11] However, in a dilute ionized gas, one may write as an approximation

$$\nu = \bar{C}_e \sum_j n_j \bar{Q}_j \tag{6}$$

where $\bar{C}_e$ is the mean thermal velocity of the electrons, n_j and $\bar{Q}_j$ are respectively the number density and velocity-averaged momentum transfer cross section for collision between an electron and the type-j particle in the ionized gas. The summation sign is to extend over all particles except the electrons.

From the above expressions, it is seen that the rate of attenuation of electromagnetic waves generally increases with the electron number density and with the gas density.

In 1956, the author has made some rough estimates of the amount of attenuation of radio frequency electromagnetic waves to be expected through the shock layer and through the wake,[14] using the above dispersion formulea and the then incomplete information concerning the properties of the hypersonic flow field. The results are reproduced here in Figs. 9, 10(a) and (b). The surprising conclusion was that even at re-entry velocity corresponding to that of long range missiles (i.e., somewhat below the satellite velocity), it appeared very difficult to overcome the"communication blackout" phenomenon during re-entry, except perhaps through the use of extremely-low or extremely-high radio frequencies. However, the basic information concerning the atomic and molecular properties of high temperature air as well as the hypersonic flow field was too incomplete and uncertain at that time to allow one to consider such estimates very quantitative. To obtain quantitative information, one needs to know again the precise thermodynamic state of the gas in the various parts of the flow field; the chemical kinetic processes which govern the rates of production and of disappearance of free electrons; the momentum transfer cross sections of the various chemical species in much the same order as in the optical communication problem.

THE PROBLEM OF SIMULATION

From the foregoing discussion it is quite clear that the problem

of communication with a spacecraft during a re-entry crosses many fields. Its solution requires a simultaneous treatment of the fluid dynamics problem, the chemical kinetics problem, and the problem of propagation of electromagnetic waves in an inhomogeneous hypersonic flow field. Because of the complexity of the problem, there naturally arises the question of whether one can obtain an analogue-type solution to the overall problem through the use of properly constructed scale model in the laboratory without going into the intermediate steps of understanding the various processes. In other words, there is a question of whether the re-entry communication problem can be easily simulated. Unfortunately, the answer seems to be discouragingly negative as far as direct simulation is concerned. The reasons are many. For one thing, the chemical kinetic processes which govern the thermodynamic and chemical properties of the flow field do not have a simple density dependence. For example, the endothermic processes which govern the dissociation and ionization rates of air in the shock compression region mainly involve binary collisions, whereas the exothermic processes which govern the atomic recombination rate and the electron attachment rate in the expansion region mostly involve ternary collisions. For binary reactions, the instantaneous rates depend on the square of the local gas density; while for termary reactions, the instantaneous rates depend on the cube of the local gas density. This is illustrated by Fig. 11, which shows the various regions in the model size versus gas density plot in which the scaling of the chemical reaction rates in the hypersonic wake is either binary, ternary, or a combination of both.[15] For another thing, in the propagation problem, the refractive index n and the extinction coeffic- ient κ not have a simple density and wavelength dependence (see Eqs.

1 through 6). Therefore, in order to obtain full simulation of all the phenomena, one must duplicate the physical dimension of the spacecraft, the free stream conditions, and the electromagnetic wavelength at the same time.

While the problem of full simulation appears very difficult, if not impossible, it is fortunate that there is a natural separation between the dynamics aspect of the hypersonic flow problem and the chemical physics aspect of the hypersonic flow problem, in the sense that the pressure and velocity distributions are relatively insensitive to the equation of state of the gas. Similarly, there also exists a natural separation between the fluid dynamics problem and the electromagnetic problem of propagation, to the extent that within limits of the electromagnetic wave power density there is very little interaction between the two phenomena. This, in effect, allows one to treat the three aspects of the problem quite separately and to carry out partial simulation whenever appropriate. Final answer to the overall problem can then be obtained through synthesis. We shall now illustrate how this can be done:

Referring again to the schematic drawing of the hypersonic flow field shown in Fig. 1, the pressure field is mostly controlled by the shape of the bow shock (see Ref. 1). Due to continuous decrease in strength of the bow shock wave away from the apex, the chemical reaction and excitation processes occur mostly in those parts of the fluid which are closest to the flight axis of the re-entering spacecraft (that is, the high enthalpy gas that has been processed by the nearly normal portion of the bow shock wave). Since the total mass of this gas is small compared with the total mass of air engulfed by

the bow shock wave, it has relatively little effect on the overall pressure field of the hypersonic flow. On the other hand, the bulk of the gas which passed through the outer and relative weak part of the bow shock wave experiences little temperature change and hence has little chemical activity. Thus, the pressure distribution throughout the hypersonic flow field can be determined quite reliably through the application of hypersonic flow theories that have been developed for perfect gases of constant specific heats.[16] From the pressure field so determined, the velocity field for the high enthalpy flow near the flight axis can in turn be determined from the (nearly one-dimensional) equation of motion. From the known pressure and velocity fields, the time history of chemical reactions following each fluid element can then be determined if all the chemical kinetic and excitation rate constants were known.[11] Knowing the distribution of chemical species in the high enthalpy flow, the electromagnetic properties of the hypersonic flow field can in turn be calculated from the atomic and molecular properties of the various chemical species. From the known distribution of electrical properties of the flow field, a final simulation of the electromagnetic propagation can be made through the use of models made of suitable dielectric or diamagnetic material which duplicate the distribution of the complex propagation constant of the flow field.

What we just proposed is in effect to subdivide the entire simulation problem into three separate parts; namely, (i) an aerodynamic simulation to determine the pressure and velocity field, using hypersonic wind tunnel or ballistic range facilities which simulate the flight Mach number and Reynolds number but not necessarily the stagnation

enthalpy corresponding to the flight condition. In this connection, existing hypersonic theories based on non-reacting perfect gases may well be utilized;[16] (ii) a chemical kinetics and atomic physics simulation, using high temperatures shock tubes or molecular beams to determine the fundamental rate constants, excitation cross sections, and other atomic and molecular properties of interest. Here, one may, of course, enlist the help of existing chemical kinetics and atomic theories whenever appropriate; (iii) an electromagnetic simulation using dielectric or diamagnetic models to study the antenna pattern if existing propagation theories prove to be inadequate.

Of the above three items, (i) is already adequately covered by Mr. Potter earlier in this session;[17] (ii) is a topic which I would like to elaborate on in a few moments; (iii) is a topic quite outside the scope of the present session.

CHEMICAL KINETICS AND ATOMIC PHYSICS SIMULATION

Within the remaining time available, I would like to view briefly the problem of chemical kinetics and atomic physics simulation. In particular, I would like to highlight some of the significant results which have been obtained from recent high temperature shock tube studies in connection with the problem under consideration.

Considering the shock compression process across the bow shock wave as a locally one-dimensional phenomenon, one can quite readily reproduce all the chemical kinetic processes in the laboratory using a high temperature shock tube. (Note that the flow across a plane oblique shock wave is equivalent to the flow across a normal shock wave with a simple

Galilean transformation in the direction tangential to the shock surface.) The operating principle of a shock tube has been adequately described in previous literatures.[18] As illustrated in Fig. 12, the basic elements of this apparatus consist of just a high pressure chamber and a low pressure chamber connected by a suitable diaphragm. When the diaphragm is ruptured, a shock wave is formed and propagates down the low pressure chamber during the early transient of the pressure equilization process. Observations can then be made of the various physical phenomena at the downstream end of the low pressure chamber through the use of suitably fast detectors. By simple variation of geometry, the shock tube can be adapted to perform quantitative experiments over wide ranges of temperature, density and chemical composition of the gas samples. With proper care, it is also possible to reduce all the undesirable effects, such as wall contamination, flow inhomogeneity, etc., to the level of small perturbations. Thus, the resultant shock-heated gas sample (that is, the region between the shock surface and the contact discontinuity in Fig. 12(b)) approaches that of an idealized one-dimensional flow behind a plane shock wave. Figure 13 shows an actual photograph of a relatively large diameter shock tube which has been constructed some time ago at the Avco-Everett Research Laboratory for chemical kinetic studies.

For simulation of the chemical kinetic processes behind a bow shock wave in flight, it is now only necessary to duplicate the shock velocity and ambient air pressure in the laboratory. Figure 14 shows the shock velocity and initial pressure ranges which are accessible to shock tubes of various types.[20] This may be compared with the velocity-density regime of interest to the flight case shown in Fig. 2. Typical

results showing the equilibrium spectral radiation intensity behind the shock wave; the ratio between the peak nonequilibrium radiation to the equilibrium radiation; the electrical conductivity of shock-heated air; some of the momentum transfer cross sections between electron and neutral atoms; the electron density distribution behind a normal shock; the peak nonequilibrium electron density; and the characteristic ionization distance behind the shock are illustrated respectively in Figs. 15 through 21. For detailed information concerning the individual experiments leading to the results just presented, the readers are referred to the referenced literature indicated in the respective figure captions.

Finally, to illustrate how the chemical kinetics information may be utilized to determine the electromagnetic property of the hypersonic flow field from a synthesis of the aerodynamics and chemical kinetics simulation, a typical plot of the free electron number density distribution in the wake of a sphere at hypersonic speed, and the absolute root-mean-square electron density flucutation in the wake, are illustrated respectively in Figs. 22 and 23. Detailed descriptions of how such synthesis was carried out may be found in Refs.15 and 23.

REFERENCES

1. L. Lees and L. Hromas, "Turbulent Diffusion in the Wake of a Blunt-Nosed Body at Hypersonic Speeds, J. Aerospace Sciences, 29, 976 (1962).

2. B. Kivel, "Radiation from Hot Air and Stagnation Heating," J. Aerospace Sciences, 28, 96 (1961).

3. L. Lamb and S. C. Lin, "Electrical Conductivity of Thermally Ionized Air Produced in a Shock Tube," J. Appl. Phys., 28, 754 (1957).

4. C. C. Petty, "Semi-Automated Reduction of Photograph in Data for Missile Re-entry," Avco-Everett Research Laboratory, AMP 138, June, 1964; also Proceedings of the Photo-Optical Data Reduction Seminar of the Society of Photo-optical Instrumentation Engineers, St. Louis, Mo., March 2-3, 1964.

5. J. D. Teare, "Ionization Behind Shock Waves," p. 217, Progress in Astronautics and Aeronautics, Vol. 12 (Ed. K. E. Shuler and J. B. Fenn), Academic Press, New York (1963).

6. L. Lees, "Hypersonic Wakes and Trails," AIAA Journal, 2, 417 (1964).

7. E. E. Salpeter and S. B. Treiman, "Backscatter of Electromagnetic Radiation from a Turbulent Plasma," J. Geophys. Res., 69, 869 (1964).

8. S. C. Lin, W. P. Goldberg, and R. B. Janney, "Radio Echoes from the Ionized Trails Generated by a Manned Satellite During Re-entry," Avco-Everett Research Laboratory, Research Report 127, April, 1962; also J. Geophys. Res., 67, 3851 (1962).

9. J. C. Keck, J. C. Camm, B. Kevel and T. Wentink, Jr., "Radiation from Hot Air, Part II," Annals of Physics, 7, 1 (1959).

10. S. K. Mitra, "The Upper Atmosphere," 2nd Ed., Chapter VI, Asiatic Society, Calcutta (1952).

11. H. Margenau, "Conduction and Dispersion of Ionized Gases at High Frequencies," Phys. Rev., 69, 508 (1946).

12. W. P. Allis and S. J. Buchsbaum, "Waves in Anisotropic Plasmas," Massachusetts Inst. of Technology Press, Cambridge (1963).

13. T. H. Dupree, "Theory of Radiation Emission and Absorption in Plasma," Phys. of Fluids, 7, 923 (1964).

14. S. C. Lin, "A Rough Estimate of the Attenuation of Telemetering Signals through the Ionized Gas Envelope around a Typical Re-entry Missile," Avco-Everett Research Laboratory, Research Report 74, February, 1956.

15. S. C. Lin and J. E. Hayes," A Quasi One-Dimensional Model for Chemically Reacting Turbulent Wakes of Hypersonic Objects," Avco-Everett Research Laboratory, Research Report 157, July 1963.

16. W. D. Hayes, and R. F. Probstein, "Hypersonic Flow Theory," Academic Press, New York (1959).

17. J. L. Potter, "Flow Fields, Pressures, Forces, Moments and Motions," Conference on the Role of Simulation in Space Technology, Virginia Polytechnic Institute, Blacksburg, Virginia, August 17-21, 1964.

18. E. L. Resler, S. C. Lin, and A. R. Kantrowitz, "The Production of High Temperature Gases in Shock Tubes," J. Appl. Phys., 23, 1390 (1952).

19. S. C. Lin, and W. I. Fyfe, "Low-Density Shock Tube for Chemical Kinetics Studies," Phys. of Fluids, 4, 238 (1961).

20. J. C. Camm and P. H. Rose, "Electric Shock Tube for High Velocity Simulation," Phys. of Fluids, 6, 663 (1963).

21. R. A. Allen, P. H. Rose, and J. C. Camm, "Nonequilibrium and Equilibrium Radiation at Super-Satellite Re-entry Velocities," Avco-Everett Research Laboratory, Research Report 156, September, 1962; also Institute of Aerospace Sciences, Preprint 63-77, (1963).

22. S. C. Lin and J. D. Teare, "Rate of Ionization Behind Shock Waves in Air, II, Theoretical Interpretation," Phys. of Fluids, 6, 355 (1963).

23. S. C. Lin, "A Partial-Dissipation Approximation for Chemical Reactions in Heterogeneous Turbulent Flows," Avco-Everett Research Laboratory, Research Report 180, April, 1964.

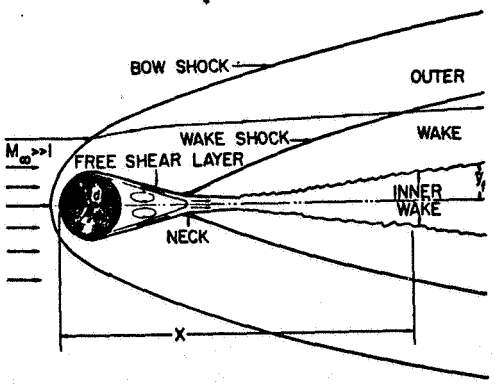

Figure 1: Wake behind blunt body at hypersonic speeds (after Lees, Ref. 1).

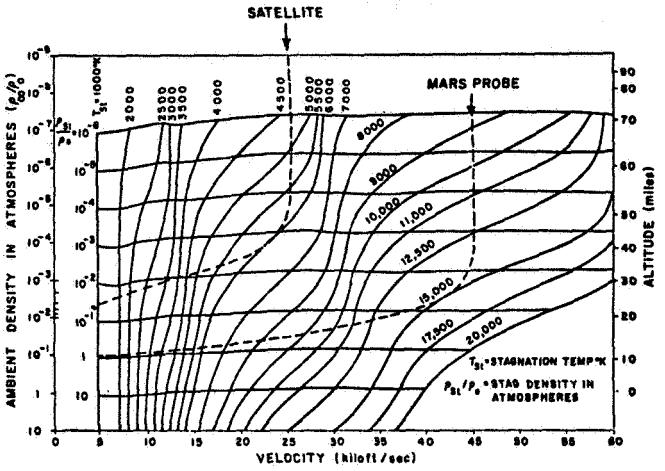

Figure 2: Stagnation temperature and density values as a function of ambient density and flight velocity.

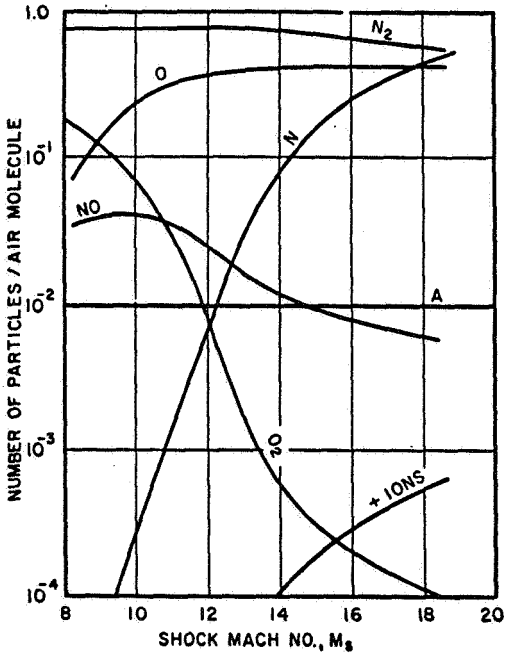

Figure 3: Composition of air behind moving shock wave as a function of shock Mach number. Initial temperature of undisturbed gas, T_1 = 293°K; initial pressure p_1 = 1 mm Hg.

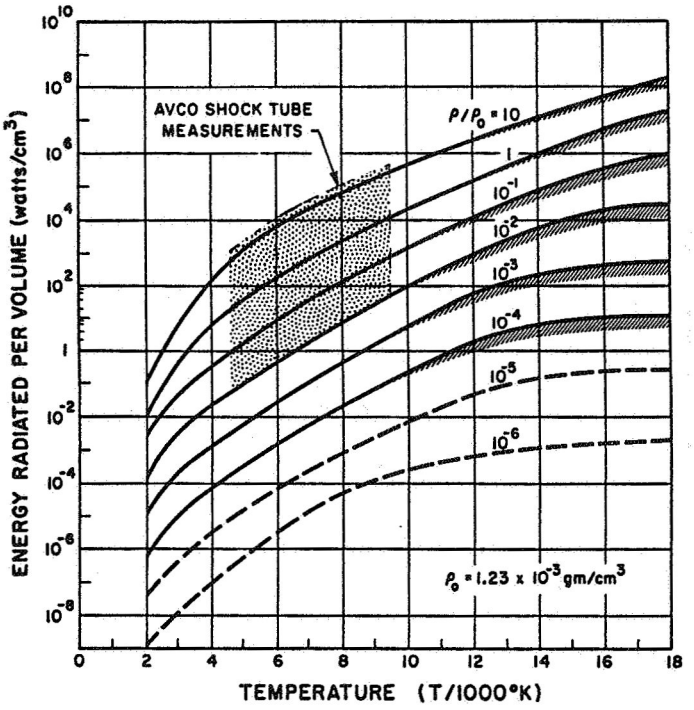

Figure 4:
Total emitted radiation energy per unit volume of high temperature air in full equilibrium as a function of temperature for constant values of the density. (see Ref. 2).

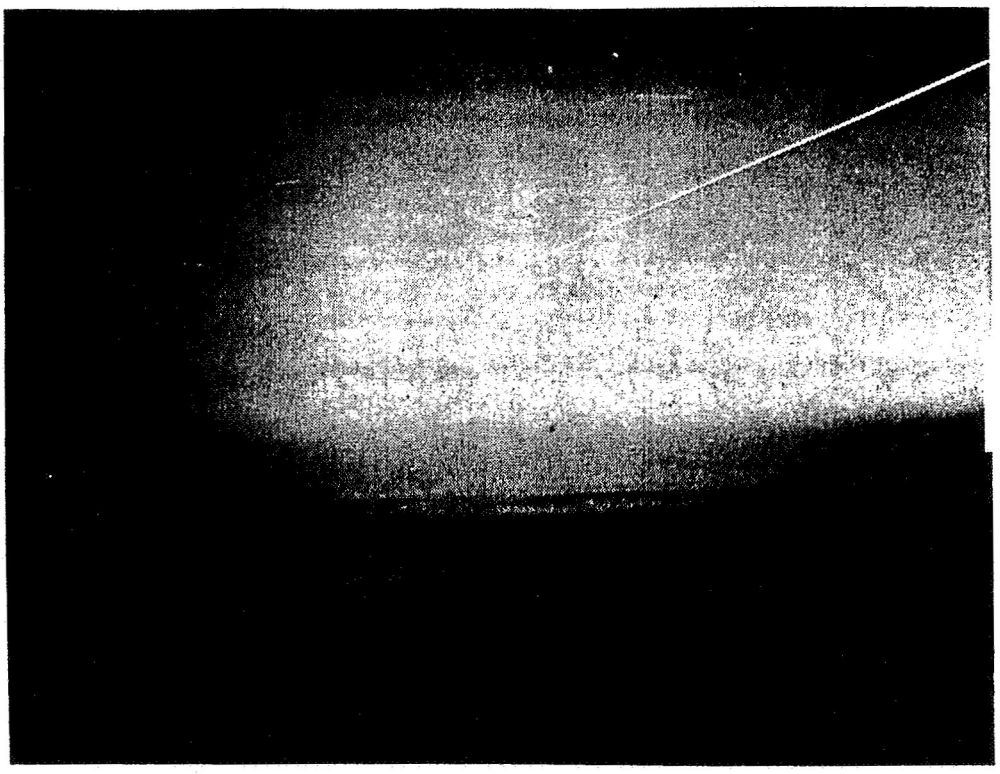

Figure 5: Ballistic camera photo of ICBM nose cone re-entry over the South Atlantic, taken by the Avco-Everett Research Laboratory Re-entry Experiments Operation (Ref. 4).

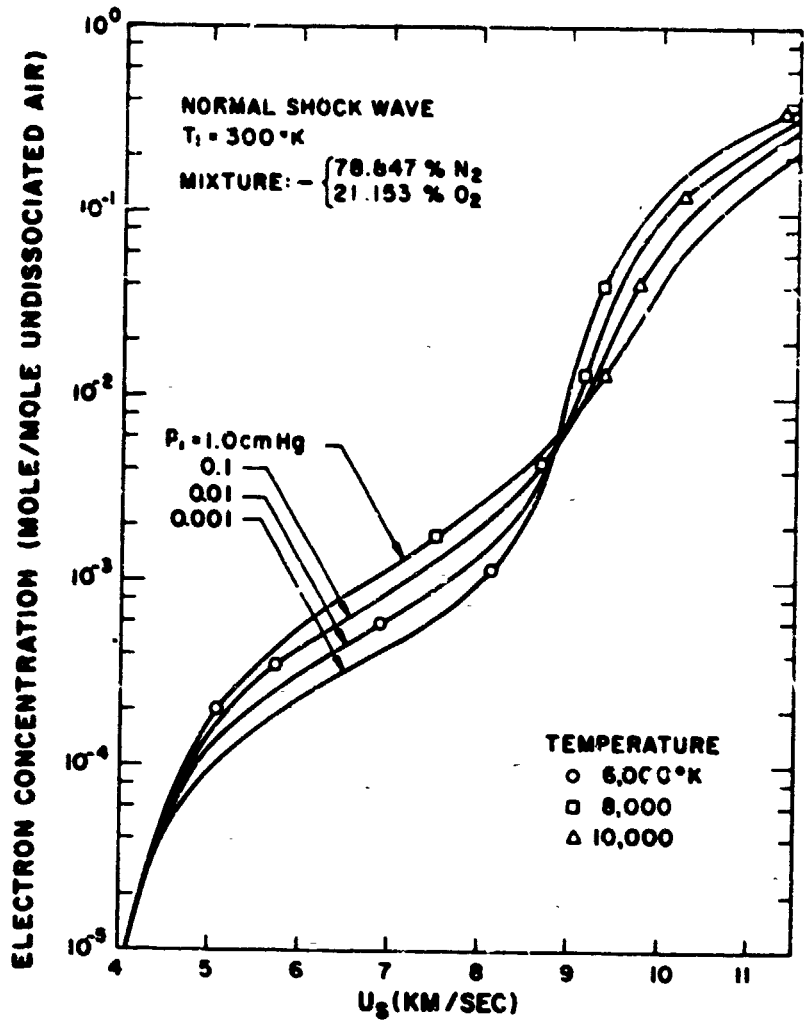

Figure 6: Equilibrium degree of ionization behind a normal shock wave in argon-free air as a function of shock velocity for a range of values of initial pressure, p_1, in the undisturbed gas. The variation of equilibrium temperature with shock speed is also shown (see Ref. 5).

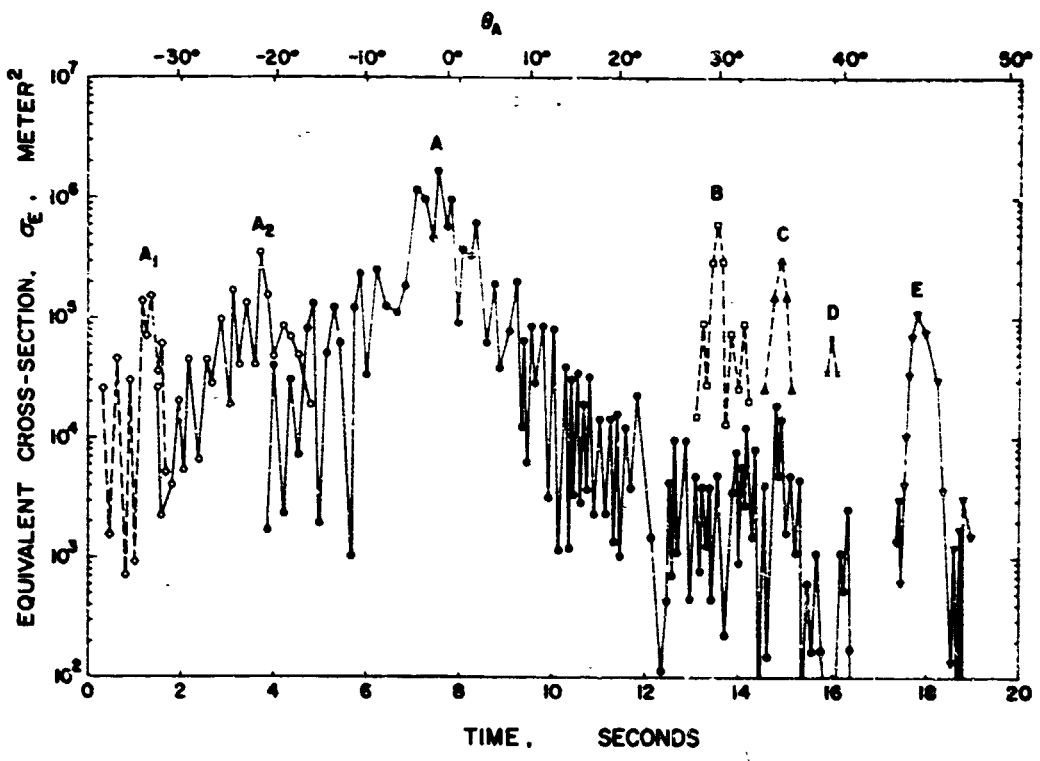

Figure 7: Back-scatter cross section of MA-6 Mercury capsule during re-entry observed by Lin, Goldberg and Janney(Ref. 9).

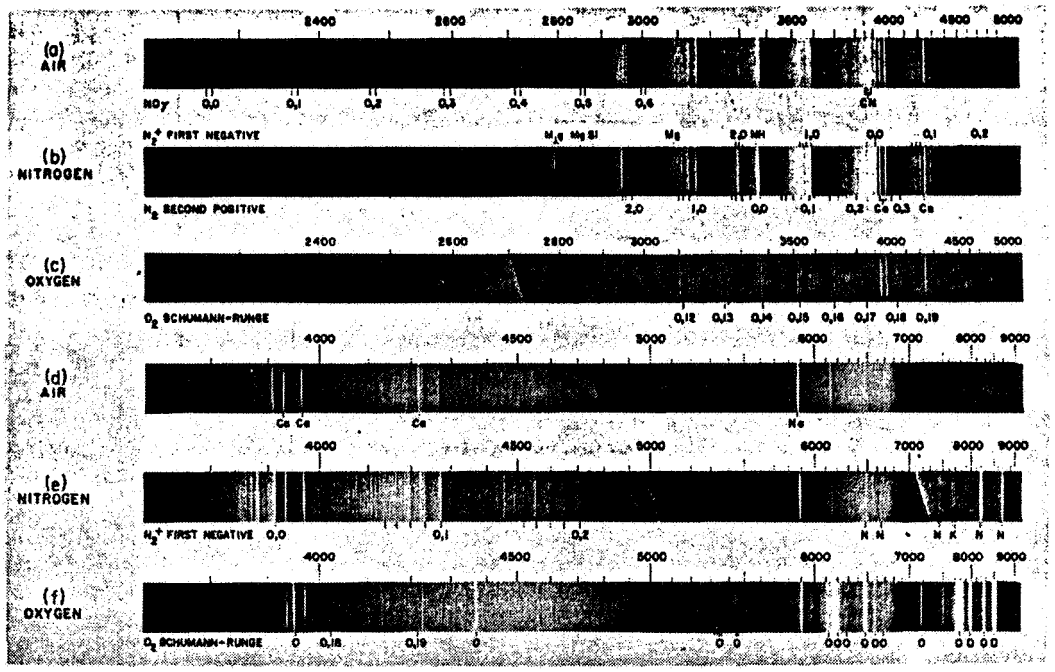

Figure 8: Shock tube spectra of high temperature air, nitrogen, and oxygen obtained by Keck, Camm, Kivel and Wentink (Ref. 9).

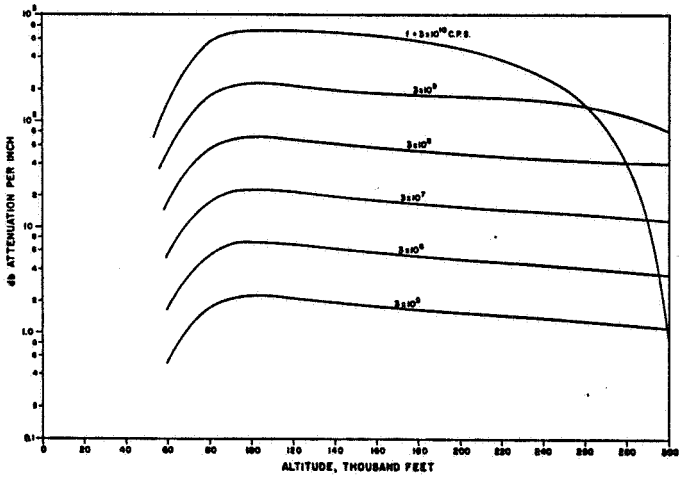

Figure 9: Attenuation of plane electromagnetic waves through the boy shock layer of a blunt body during re-entry (Ref. 14).

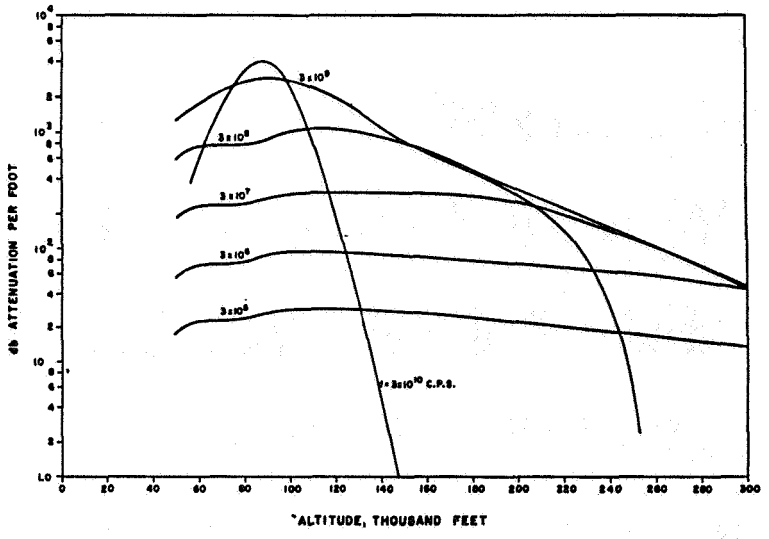

Figure 10(a): Attenuation of plane electromagnetic waves through the wake of a blunt body during re-entry for equilibrium ionization (Ref. 14).

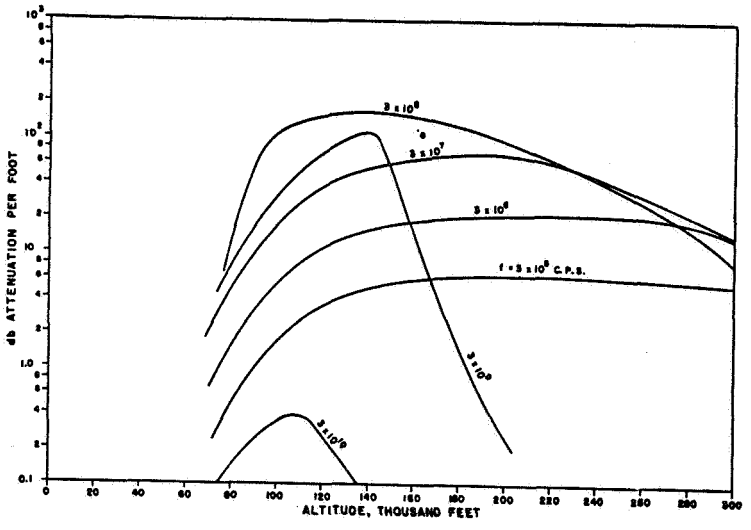

Figure 10(b): Attenuation of plane electromagnetic waves through the wake of a blunt body during re-entry for frozen ionization (Ref. 14).

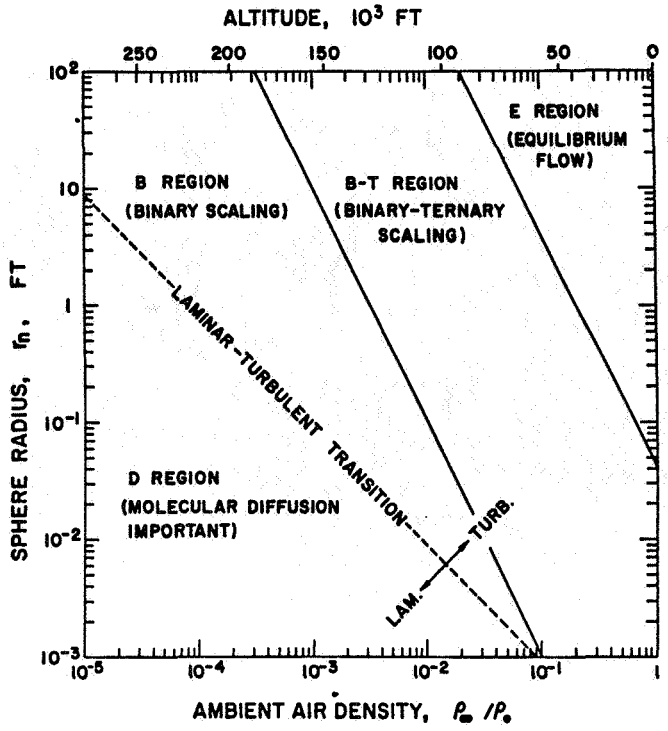

Figure 11: Approximate boundaries for scaling of chemically reacting hypersonic flow field behind spheres at 22,000 Ft/sec velocity in air (See Ref. 15).

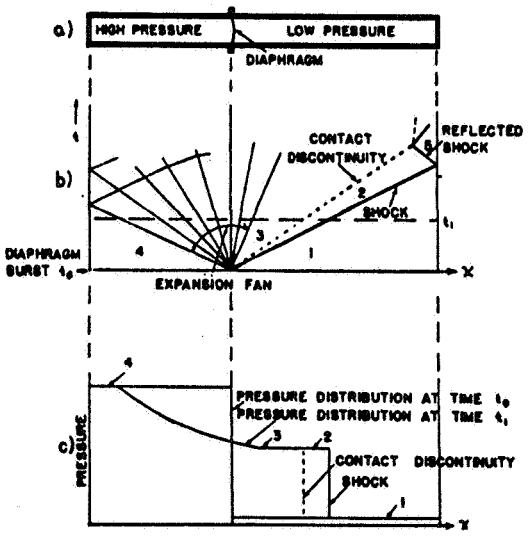

Figure 12(a): Schematic drawing of a conventional shock tube
(b): x-t diagram showing the progress of shock and expansion waves following the diaphragm burst. The gases which were originally in the high and low pressure portions of the shock tube are separated by the contact discontinuity.
(c): The pressure distribution along the shock tube at times t_0 and t_1.

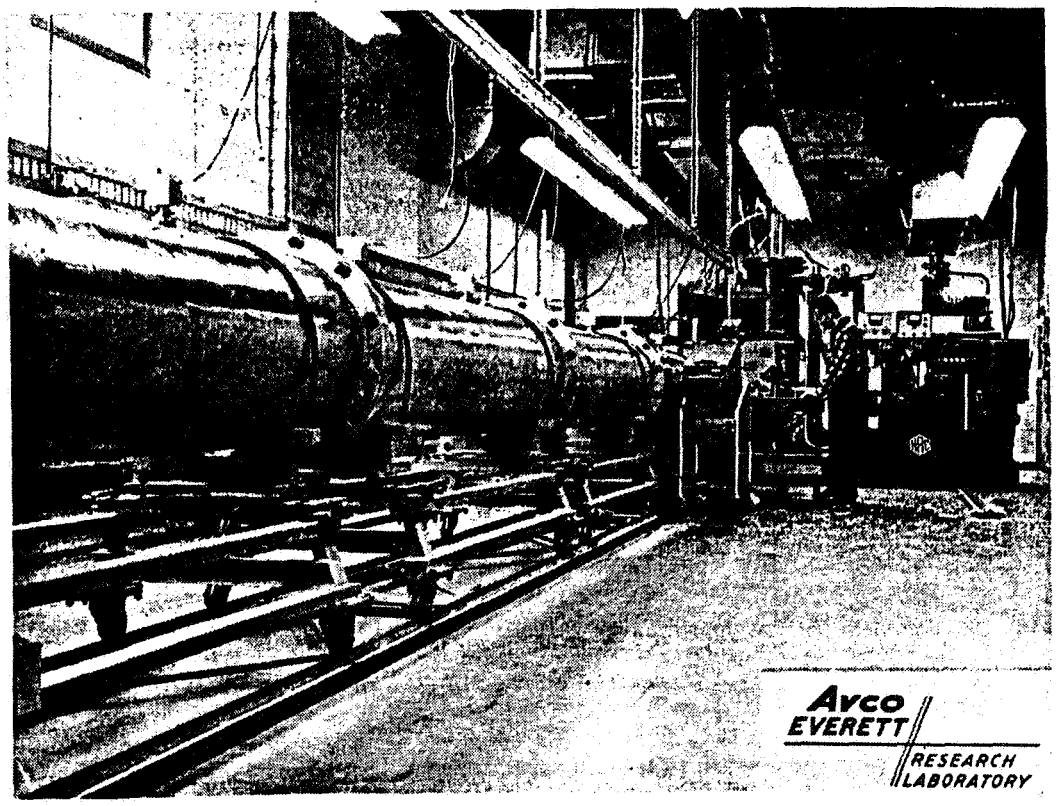

Figure 13: Photograph of a 24" diameter shock tube at the Avco-Everett Research Laboratory (see Ref. 19).

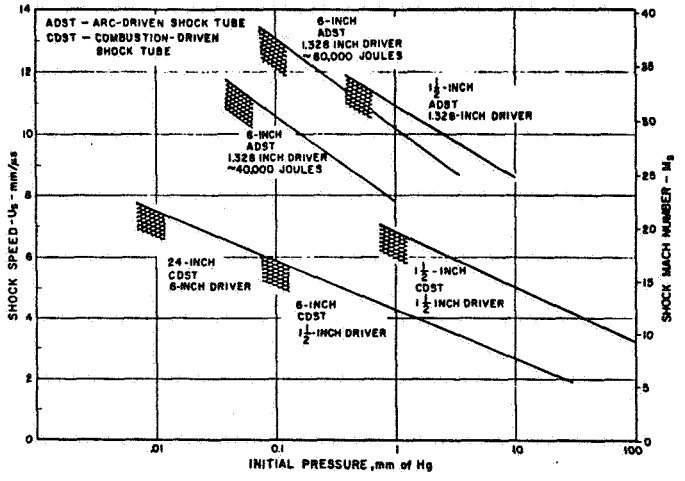

Figure 14: Approximate performance limits experienced for shock tubes presently in use. The combustion-driven shock tubes (CDST) are limited by a 10,000 psi driver pressure, and low density test time limitation depending on diameter. The arc-driven shock tubes (ADST) are limited by the energy density available in the driver, the expansion ratio between the driver and driven sections, and the test time limitation (after Camm and Rose, Ref. 20).

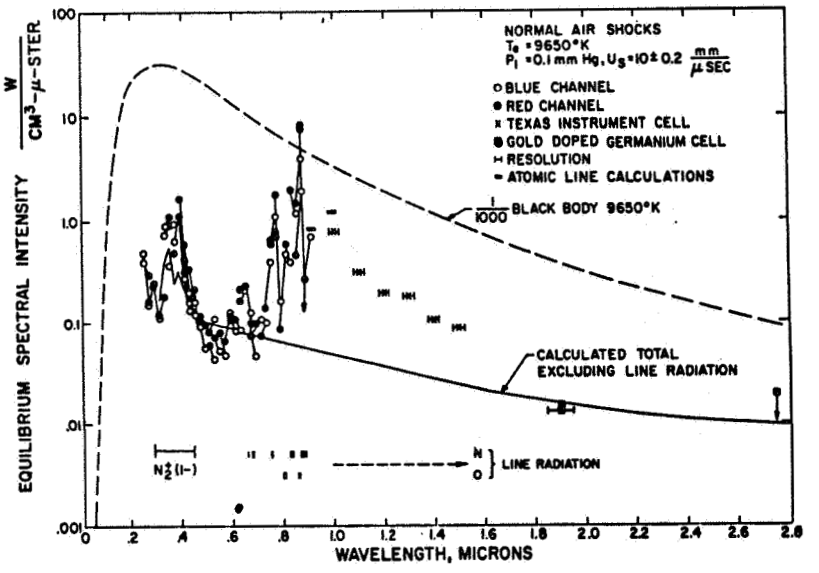

Figure 15: Equilibrium radiation data obtained by photomultipliers and infrared gauges versus wavelength obtained on incident air shocks U_s = 10 mm/μsec, P_1 = 0.1 mm Hg. The degree of ionization is about 10% (after Allen, Rose and Camm, Ref. 21).

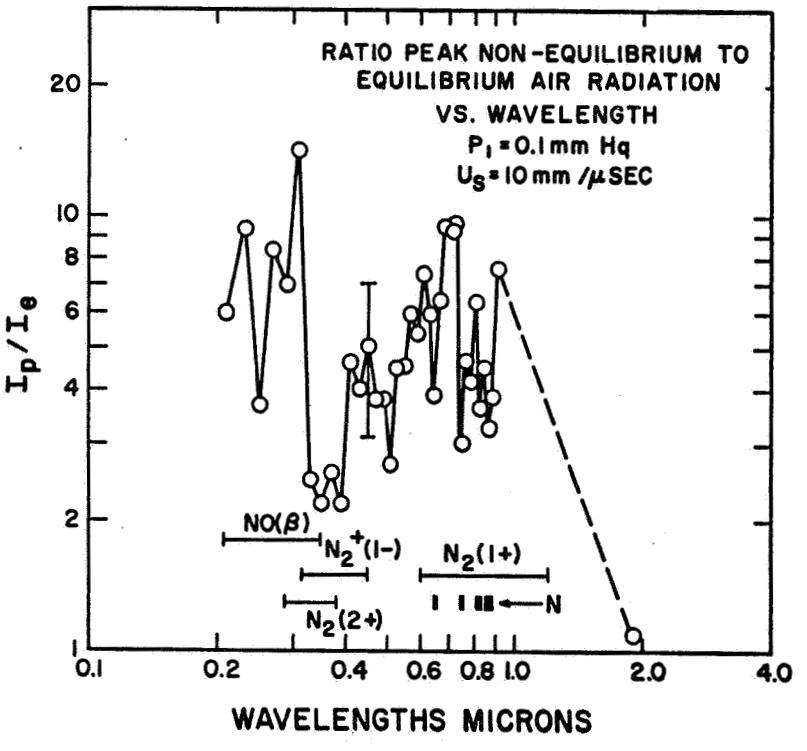

Figure 16: Ratio of peak non-equilibrium radiation to equilibrium radiation versus wavelength at super-satellite velocity according to Allen, Rose and Camm (Ref. 21).

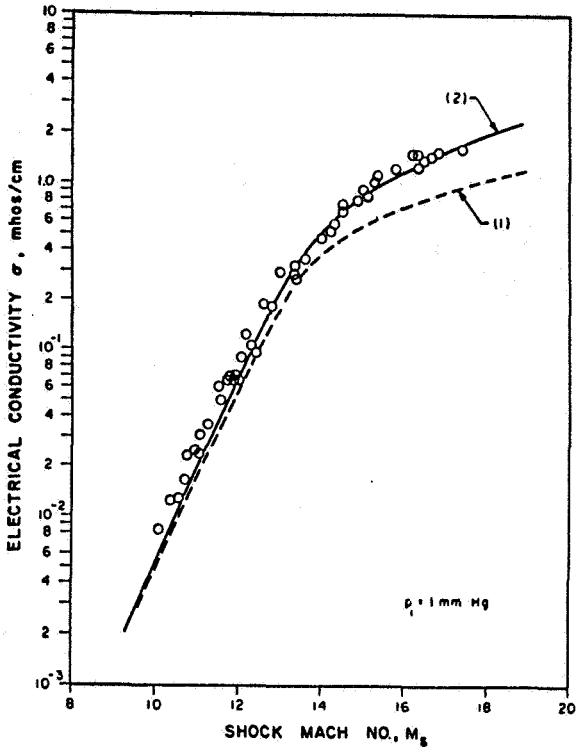

Figure 17: Comparison between experimental and theoretical electrical conductivity of air behind normal shock wave (see Ref. 3).

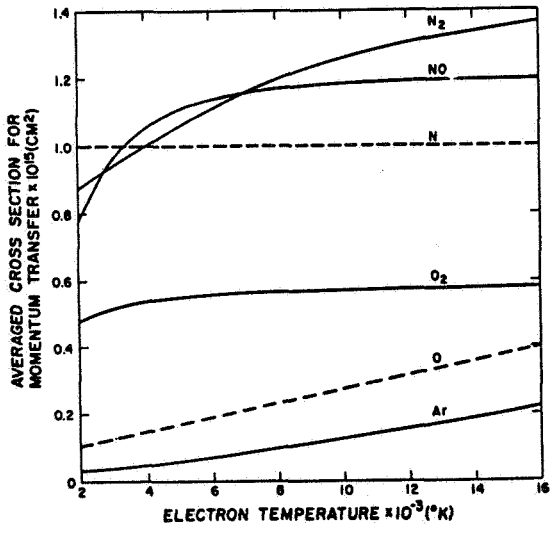

Figure 18: Velocity-averaged cross sections for momentum transfer between electrons and the various neutral components of high temperature air, as functions of electron temperature (see Ref. 5).

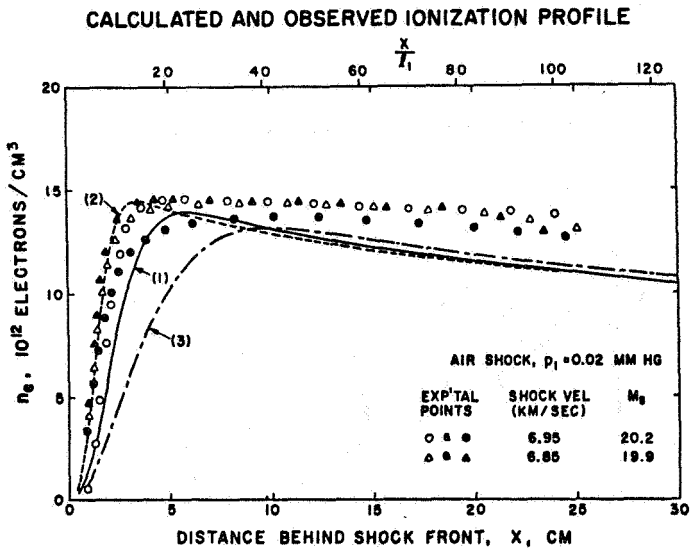

Figure 19: Comparison between calculated and observed electron density distributions behind the shock for the case $U_s = 6.9 \pm 0.05$ km/sec and $P_1 = 0.02$ mm Hg. (See Ref. 22).

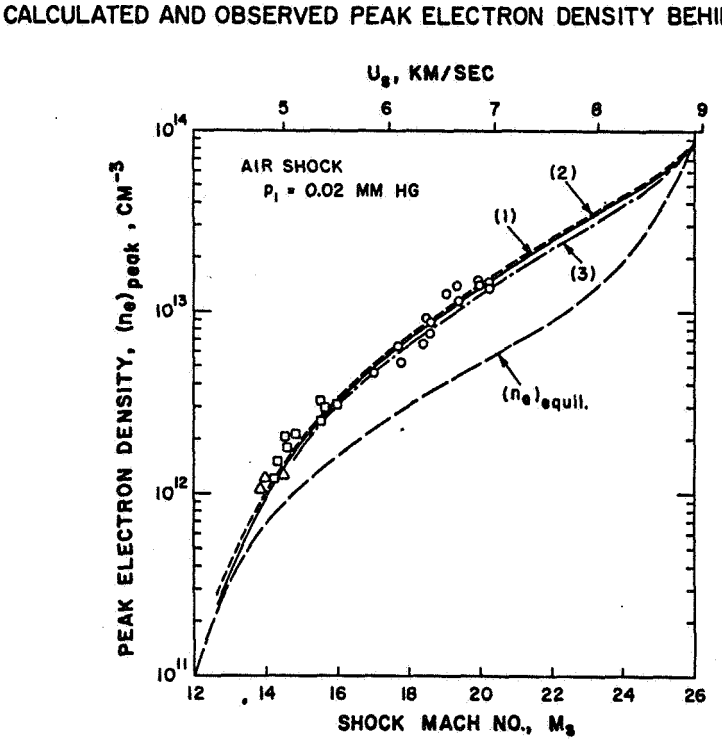

Figure 20: Comparison between calculated and observed peak electron density behind the shock as a function of shock velocity at $P_1 = 0.02$ mm Hg (see Ref. 22.).

CALCULATED AND OBSERVED IONIZATION RISE DISTANCE

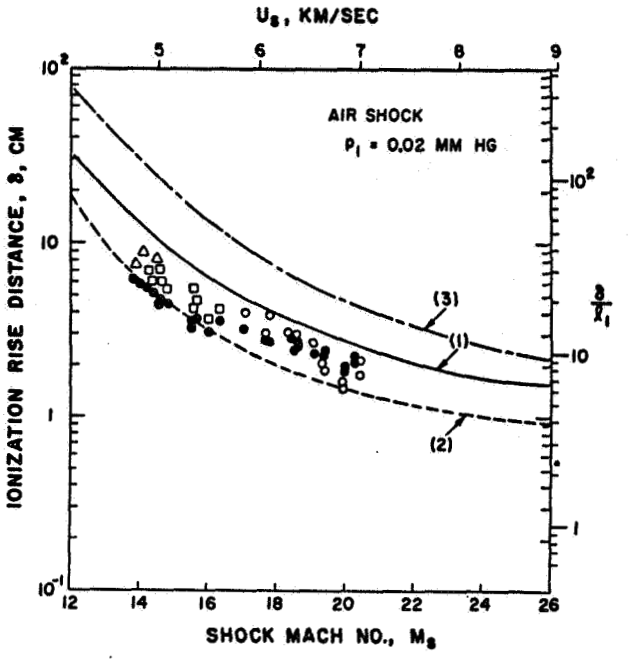

Figure 21: Comparison between calculated and observed ionization rise distance behind the shock as a function of shock velocity at P_1 = 0.02 mm Hg (see Ref. 22).

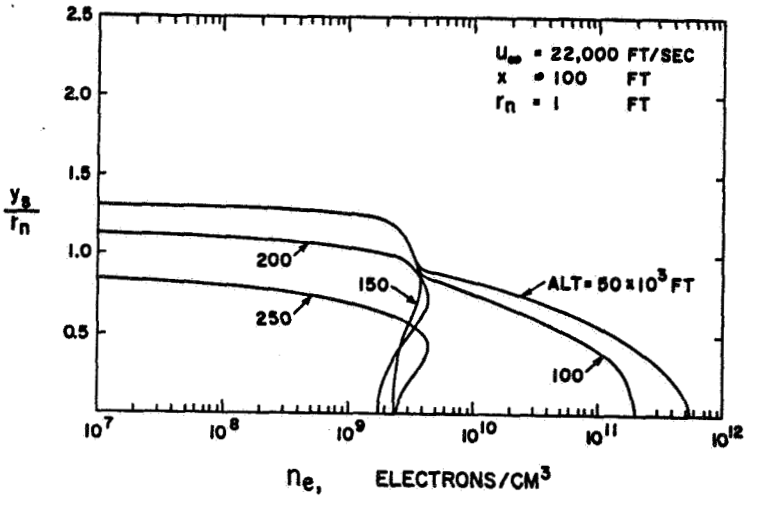

Figure 22: Radical distribution of electron density in a hypothetical axisymmetric, laminar, inviscid, but chemically reacting hypersonic wake behind a sphere of 1 ft. radius at 22,000 ft/sec velocity and at ambient density corresponding to the various indicated altitudes (see Ref. 15).

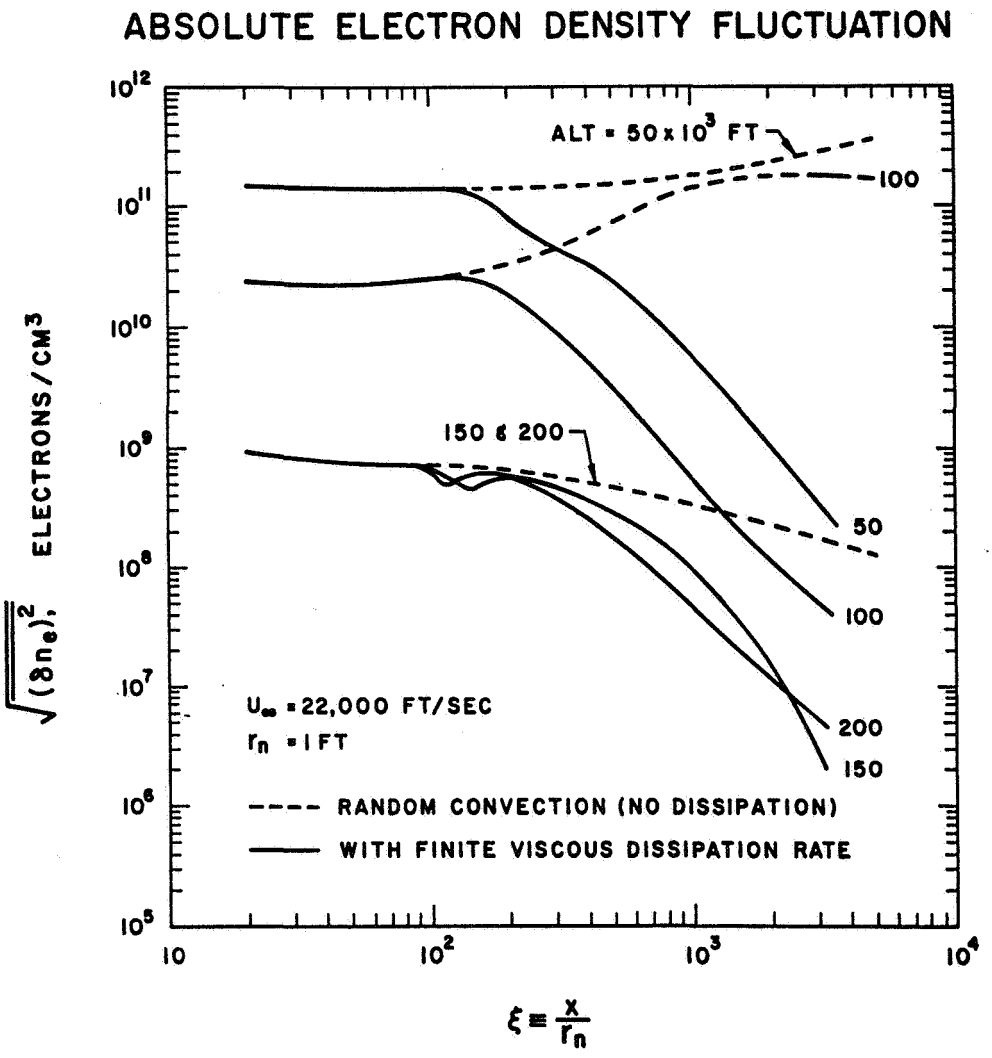

Figure 23: Absolute root-mean-square electron density fluctuation in a quasi one-dimensional turbulent wake behind a hypersonic sphere (see Ref. 23).